Non-oxidized graphene/metal composites by laser deposition additive manufacturing

Wang, T., Meng, Q., Araby, S., Yang, G., Li, P., Cai, R., Han, S. & Wang, W.

Author post-print (accepted) deposited by Coventry University's Repository

Original citation & hyperlink:
Wang, T, Meng, Q, Araby, S, Yang, G, Li, P, Cai, R, Han, S & Wang, W 2021, 'Non-oxidized graphene/metal composites by laser deposition additive manufacturing', Journal of Alloys and Compounds, vol. 882, 160724.
https://dx.doi.org/10.1016/j.jallcom.2021.160724

DOI 10.1016/j.jallcom.2021.160724
ISSN 0925-8388

Publisher: Elsevier

© 2021, Elsevier. Licensed under the Creative Commons Attribution-NonCommercial-NoDerivatives 4.0 International
http://creativecommons.org/licenses/by-nc-nd/4.0/

Copyright © and Moral Rights are retained by the author(s) and/ or other copyright owners. A copy can be downloaded for personal non-commercial research or study, without prior permission or charge. This item cannot be reproduced or quoted extensively from without first obtaining permission in writing from the copyright holder(s). The content must not be changed in any way or sold commercially in any format or medium without the formal permission of the copyright holders.

This document is the author's post-print version, incorporating any revisions agreed during the peer-review process. Some differences between the published version and this version may remain and you are advised to consult the published version if you wish to cite from it.

Non-oxidized graphene/metal composites by laser deposition additive manufacturing

Tianqi Wang[1], Qingshi Meng[1,2*], Sherif Araby[3], Guang Yang[1*], Pengxu Li[1], Rui Cai[4], Sensen Han[2], Wei Wang[1]

[1] Key Laboratory of Fundamental Science for Aeronautical Digital Manufacturing Process, Shenyang Aerospace University, 37 Daoyi South Avenue, Shenyang, Liaoning 110136, China

[2] College of Aerospace Engineering, Shenyang Aerospace University, 37 Daoyi South Avenue, Shenyang, Liaoning 110136, China

[3] School of Engineering and Digital Sciences, Nazarbayev University, Nur-Sultan 010000, Kazakhstan

[4] School of Mechanical, Aerospace and Automotive Engineering, Coventry University, Coventry CV1 2JH, United Kingdom

[*]Corresponding Authors: Qingshi Meng and Guang Yang

Email:mengqingshi@hotmail.com and yangguang@sau.edu.cn;

Abstract

Graphene-based metallic nanocomposites are promising materials for applications where tailored strength and functionality are required such as space and automotive industries. Additive manufacturing, specifically 3D printing, is currently considered a revolutionary process to tailor and engineer materials for certain applications. Herein, we report fast and reliable approach to prepare mechanically robust, ductile and high thermally conductive graphene-based aluminum nanocomposites using laser deposition manufacturing (LDM). Conventional ball milling was used to homogenously mix graphene platelets and aluminum alloy powder ($AlSi_7Mg$) and then sintered by LDM. Structure-property relations of aluminum/graphene nanocomposites were investigated and thus LDM process was assessed. This includes morphological characterizations such as optical microscopy, transmission electron microscopy, x-ray diffraction and energy dispersive spectrometry; and mechanical properties measurements including tensile test and Vickers hardness. The 3D printed Al-alloy/graphene nanocomposites showed increments of 60.7%, 23.03%, 193.7% and 66% in tensile strength, Young's modulus, elongation at break and Vickers hardness in comparison with pure Al-

alloy. This study proved reliability of 3D printing metallic composites with mechanical robustness and other tailored functionality such as thermal conductivity.

Key words: Graphene; Metal matrix composites (MMCs); laser deposition manufacturing (LDM); Mechanical properties

1. Introduction

Aluminum (Al) and its alloys are the most commonly used nonferrous metals in manufacturing due to their relatively low density, high specific strength, excellent electrical and thermal conductivity, low coefficient of thermal expansion and high corrosion resistance. This justifies the wide range of applications for aluminum alloys in aerospace, defence, constructions and home appliances industries. However, Al alloys suffer from low mechanical properties in comparison to steel alloys and they are poor in wear resistance. Therefore, Al composites containing spectrometer reinforcing fillers were used to address the drawbacks of pure Al. Reinforcing fillers such as alumina particles, silicon carbide and boron nitride were well investigated and commercially used in Al matrix in the last two decades [1-4]. However, aluminum composites reinforced by ceramic particles suffer from low ductility. Recently, after they succeeded in polymer nanocomposites [5-8] and ceramic composites [9, 10], carbon nanomaterials attracted significant attention in developing metal nanocomposites which possess not only high mechanical performance but also excellent physical properties such as thermal and electrical conductivity.

Graphene– single-atom thickness, plate-like material– is the strongest material ever measured (Young's modulus of 1 TPa, strength of 130 GPa) and has outstanding electron mobility at room temperature (15000 $cm^2/V{\cdot}s$) and excellent thermal conductivity (4840–5300 W/m·K) [7, 8, 11-14]. The combination of these superb properties qualifies graphene to be used in a wide range of

applications from drug delivery, energy storage devices and chemical sensors to flexible electronics and automotive-body structures. Due to the challenges in producing single layer graphene, few-layer graphene or graphene platelets is well-accepted in developing polymer nanocomposites [7]. Graphene and its derivatives – graphene oxide, reduced graphene oxide and graphene platelets – were reported as functional and reinforcement fillers in Al matrix composites [1, 15-25]. To incorporate graphene into Al matrix, conventional preparation methods were used including–to name a few– friction stir processing, ball-milling then pressing and extrusion, ball-milling then consolidation followed by sintering, and powder metallurgy then pressing and consolidation followed by extrusion. In most of these methods, the fabrication steps could be conducted either at room temperature or high temperature [1]. Li *et al* [19] reported 36.8% increase in ultimate tensile strength of Al when 0.2 wt% of graphene platelets added to Al prepared by combination of ball milling, cold pressing, continuous casting and subsequent rolling. Despite of the outstanding mechanical and physical properties of graphene, the reported enhancements in Al/graphene composites are below the expected outcomes and even accompanied with reduced ductility. The main reasons are (i) the phase separation due to poor wettability of graphene with most of metal matrices; (ii) the nonuniform dispersion of graphene (in general nanofillers) in the Al matrix; clustering and agglomeration of nanofillers at solid/liquid interface during solidification, and (iii) the formation aluminum carbide (Al_4C_3) at the interface which promotes the phase separation and reduces the mechanical performance.

Additive manufacturing– or (3D printing)– becomes one of the fastest growing technology in digital manufacturing where a complete part can be fabricated directly in layer-bay-layer technique from a computer-aided design (CAD) file. Powder-based 3D printing methods including laser deposition manufacturing (LDM) and selective laser melting (SLM) offer design flexibility and high product

quality [26]. Inspired by the successfulness of 3D printing in developing end-product from polymer nanocomposites, it starts to attract attention to employ it in metal matrix composites. Hu's group reported promising results of 3D printed metal-matrix nanocomposites [27-30]. In a recent study, Hu *et al* [28] prepared Al/graphene platelets nanocomposites using 3D printing technology. Graphene platelets and aluminum powder were first mixed by ball-milling then sintered by the SLM method; 2.5 wt% of graphene platelets improved Vickers hardness of Al by 75.6%. By looking at the published studies on metal-matrix composites prepared by 3D printing, clear procedures and efficiency of the fabrication process, and structure-property relations of the end-product still need more in-depth investigation.

In the current study, aluminum alloy ($AlSi_7Mg$) was used as matrix and graphene platelets were added *via* laser deposition manufacturing (LDM) process to produce Al/GnP nanocomposites. To the best of our knowledge, LDM method is reported here for the first time to prepare Al/graphene platelets. The reported results show that the Al alloy not only has gained outstanding enhancements in Young's modulus and ultimate tensile strength by adding GnPs but also they possess high ductility which was always challenge the maintain in previous works.

2. Experimental procedures

2.1. Powder materials

An atomized aluminum alloy ($AlSi_7Mg$) in powder form with size range 63–150 μm was employed in this study; its elemental analysis is shown Table 1. Aluminum alloy powder was purchased from *Kangpu Xiwei* Technology Co., Ltd, Beijing**,** Graphite intercalation compounds (GICs) 1395 were kindly supplied by Asbury Carbon (Asbury, NJ, USA).

No-oxidized graphene platelets were fabricated by thermally shocking GICs; 0.5 gram of GICs were

transferred to a preheated crucible at 700℃ for one minute in a muffle furnace. After that, the expanded product was added into a beaker filled with alcohol for at least 2 hours of ultrasonication. Finally, the produced graphene platelets (GnPs) were dried overnight in a fan oven at 80℃. Vertical planetary ball milling machine (YXQM-2L, Changsha MITR Instrument and Equipment, China) was used to homogenously wrap and/or attach the produced GnPs onto the surface of aluminum alloy ($AlSi_7Mg$) powder. The aluminum alloy powder, GnPs and moderate amount of alcohol were added and sealed in a stainless-steel tank which contains 5mm diameter stainless steel balls for ball-milling process. The ball-milling process was running at 260 rpm for 16 hours under vacuum; the process stopped 5min break every 30 mins to avoid excessive heating. The mass ratio of Al-alloy powder to steel balls was 1:5 which represents volume ratio of 1:2 considering density of aluminum and steel as 2.7 and 7.7 g/cm^3, respectively. Aluminum alloy/GnP composites at fractions 0.05, 0.1 and 0.2 wt% were prepared. Pure aluminum alloy powder was ball-milled under the same conditions as a control sample. The fabrication process is schematically presented in Figure 1.

Table 1. Elemental analysis of aluminum alloy $AlSi_7Mg$ in wt%

Si	Mg	Ti	Be	Al
6.5-7.5	0.45-0.60	0.10-0.20	0.05-0.07	Balance

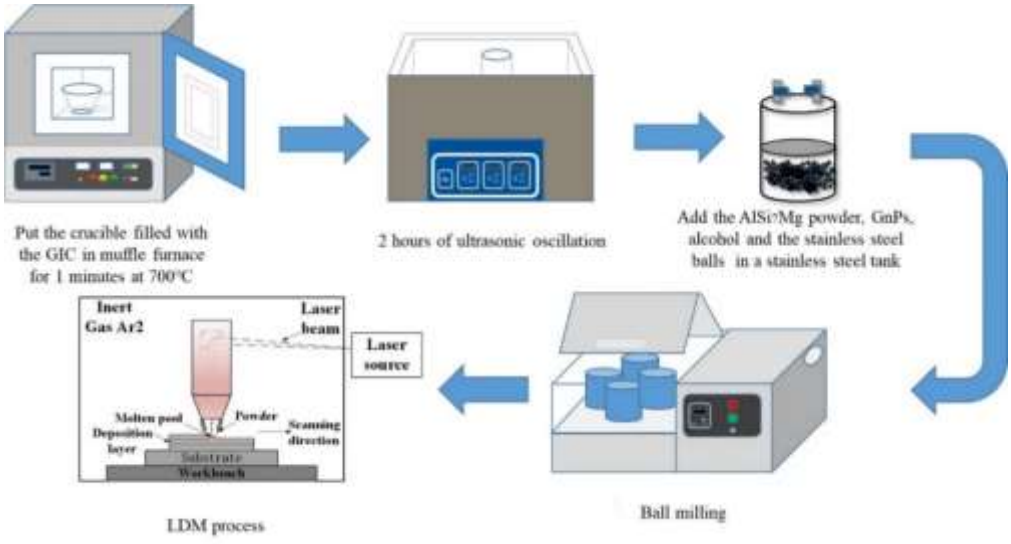

Figure 1. Schematic diagram for 3D printing Al- alloy/GnP nanocomposites by LDM

2.2. Laser deposition manufacturing process

The laser deposition manufacturing (LDM) process was carried out using LDM-800 system which is a home-customized system. Figure 1 shows a schematic illustration of LDM process. It consisted of 6 kW-semiconductor laser (wave length 1064nm) at frequency 50 kHz, pneumatic feeder and four equipped with water-cooling system.

The deposition head of the LDM machine moves following to a G-M code generated by a CAD file; the head is operated by a computer numerical control (CNC) system in 3 axes. The laser beam is coaxial with the deposition head providing an accurate movement along the designed trajectory based on the 3D-CAD file. The heat energy provided by laser beam selectively melts the GnP-coated metal particles forming a molten pool which starts to solidify once the beam moves away. The selectively melting process with the CNC motion was repeated until a neat-net shape product is built using layer-by-layer approach [31, 32]. The LDM process was carried out at the following parameters: laser intensity (1900W), laser spot diameter (4mm), scanning speed (5mm/s) with step rate (50%) and powder feed rate (0.6 rev/min)[33]. The laser head was fixed on computer numerical controlled x-y stage. A flat substrate from Al alloy ($AlSi_7Mg$) was polished and cleaned and used as platform for Al/GnP composites. The LDM process was performed in closed chamber filled with argon gas to prevent oxidation during manufacturing. Al composites with 0, 0.05 and 0.1 wt% GnPs were 3D printed. Cubic specimens of size 15×15×10mm were prepared for microstructure analysis. Flat-dumbbell samples of dimensions 70×18×5mm were 3D printed and used for tensile testing.

2.3. Characterizations

2.3.1 Morphology of GnPs and Al alloy powders

Transmission electron microscopy (TEM) was used to observe the morphology of graphene platelets

(GnPs). 0.1g GnPs was added into a beaker with 100ml alcohol and ultrasonicated for 30 min. 10% of the liquid was then extracted and added to 100ml of alcohol for another 30 min of ultrasonication. This process was repeated till 0.0004% concentration of GnPs was obtained. Few droplets of 0.0004% GnPs suspension were dropped on 200-mesh copper grids, dried and observed by transmission electron microscope (TEM-JEM-2100, JEOL, Japan) with 200kV of accelerating voltage. Further investigation was conducted to measure GnP's thickness by atomic force microscope (AFM, Dimension FastScan, Bruker, Germany) using the same 0.0004% GnP suspension.

Scanning electron microscopy was employed to study the surface morphology of ball-milled powders of (i) pure Al alloy and (ii) Al alloy/GnP nanocomposite. The powder dispersed on a sticky conductive tape and then inserted into scanning electron microscopy (SEM, Gemini-SEM 300, Carl Zeiss, Germany). Images at various magnifications were captured at accelerating voltage of 2kV and using SE2 detector and InLens detector.

2.3.1 Morphology and mechanical performance of LDM-processed Al-alloy/GnP nanocomposites

Specimens were cut by wire electrical discharge machining from samples manufactured by LDM process and used to conduct various characterizations including microstructure morphology and mechanical performance. In microstructure measurements, specimens with dimensions of 15×15×10mm were sequentially ground by a range of SiC-abrasive papers (240# –2000#). The last polishing pass was performed by a diamond abrasive paper then the specimens were etched by a mixture of 10ml HF and 100ml H_2O. The etched surfaces were investigated by various tests such as optical microscopy, transmission electron microscopy (TEM) and x-ray diffraction (XRD). GX51

optical microscope (OM, Olympus Corporation, Japan) was used to perceive an overall image of the pure Al alloy and its GnP nanocomposite (manufactured by LDM). JEOL Jem-2100 transmission electron microscopy was used to observe the sub-micro morphology of the Al alloy and GnP Al alloy manufactured by LDM-3D printing. Phase identification was tested by XRD using an x-ray diffractometer (XRD-7000s, Shimadzu Corporation, Japan) equipped with Cu Kα radiation at 40kV and 40mA. The scan speed was set at 2°/min with 2θ range 5– 100°.

Raman spectra were obtained by a HORIBA LabRAM HR Evolution Raman spectrometer; A 532nm He-Ne laser was focused by an Olympus 50× objective as an excitation source at the centre of the sample at room temperature. Energy dispersive spectrometry (EDS, Oxford Instruments, UK) was used to determine the constituent elements of the prepared Al/GnP composites.

Mechanical performance was assisted by Vickers-type hardness and tensile test. Vickers hardness was measured by HVS-100A digital micro hardness tester operating at 200g load for 10s dwell time; ten indentations with 1mm space were measured and averaged for each specimen.

Dumbbell-shaped tensile testing samples were machined from a rectangular specimen manufactured by LDM. Dumbbell samples were profiled to gauge length of 25mm and cross-section of 10×2mm according to GB/T 228.1-2010 Standard. Tensile testing was carried out by universal tensile testing machine (MTS, China) at room temperature and crosshead speed of 2mm/min. The test was repeated three times at least for each fraction; the recorded data is the average of the measurements. The fracture surfaces after the test were further investigated by SEM.

3. Results and discussion

3.1. Morphology of graphene platelets (GnPs)

The microscopic images of the prepared graphene platelets are displayed in Figure 2a&b at high and

low magnifications; respectively image (a) and (b). Image (a) shows wrinkled and overlapped platelets stacked together. Image (b) is a high magnification of an area from Image (a) which depicts that graphene platelets consists of few layers staked and indicated by red arrows. Herein, the GnPs were prepared by thermal expansion then ultrasonication for 2 hours. Due to thermally shocking GIC at 700℃, gasses burst at high pressure providing swollen and expanded GIC that has worm-like structure where graphene layers bonded together by the weak van der Waal bonds. Ultrasonication process breaks the weakly bonded worm-like structure into few layers of graphene; graphene platelets (GnPs). A randomly selected area was examined to study the electron diffraction (ED) pattern of GnPs. The inset diffraction in Figure 2(b) confirms the high crystalline structure of the prepared graphene platelets. Both TEM images and ED agree with the previous studies [6, 34, 35].

Thickness of GnPs was measured *via* AFM by randomly selecting at least ten GnPs. Figure 2c&d shows three representative measurements recording an average thickness of 3.2 ± 0.7nm which is consistent with the previous studies [6, 35, 36]. To quantify structural integrity of GnPs, Raman spectroscopy was performed and analysis is displayed in Figure 2e. The GnPs' spectrum shows three characteristic bands at 1350, 1580 and 2716 cm^{-1} corresponding to D, G and 2D-bands respectively. The G-band is due to the in-plane stretching vibrations of sp^2 carbon atoms whereas the D-band originates due to the breathing modes of sp^2 carbon rings[37]. In general, D-band corresponds to structural defects and thus its intensity is proportional to amount of disorder or defects. Usually, the ratio between the intensities I_D/I_G is a parameter to quantify the structural integrity or disorder of graphene [38]. Herein, the I_D/I_G of GnPs is determined at 0.049 demonstrating high structural integrity GnPs in comparison with graphene oxide which is well-known by high defect concentration graphene derivative; its I_D/I_G is ~1 endowing electrically nonconductive material.

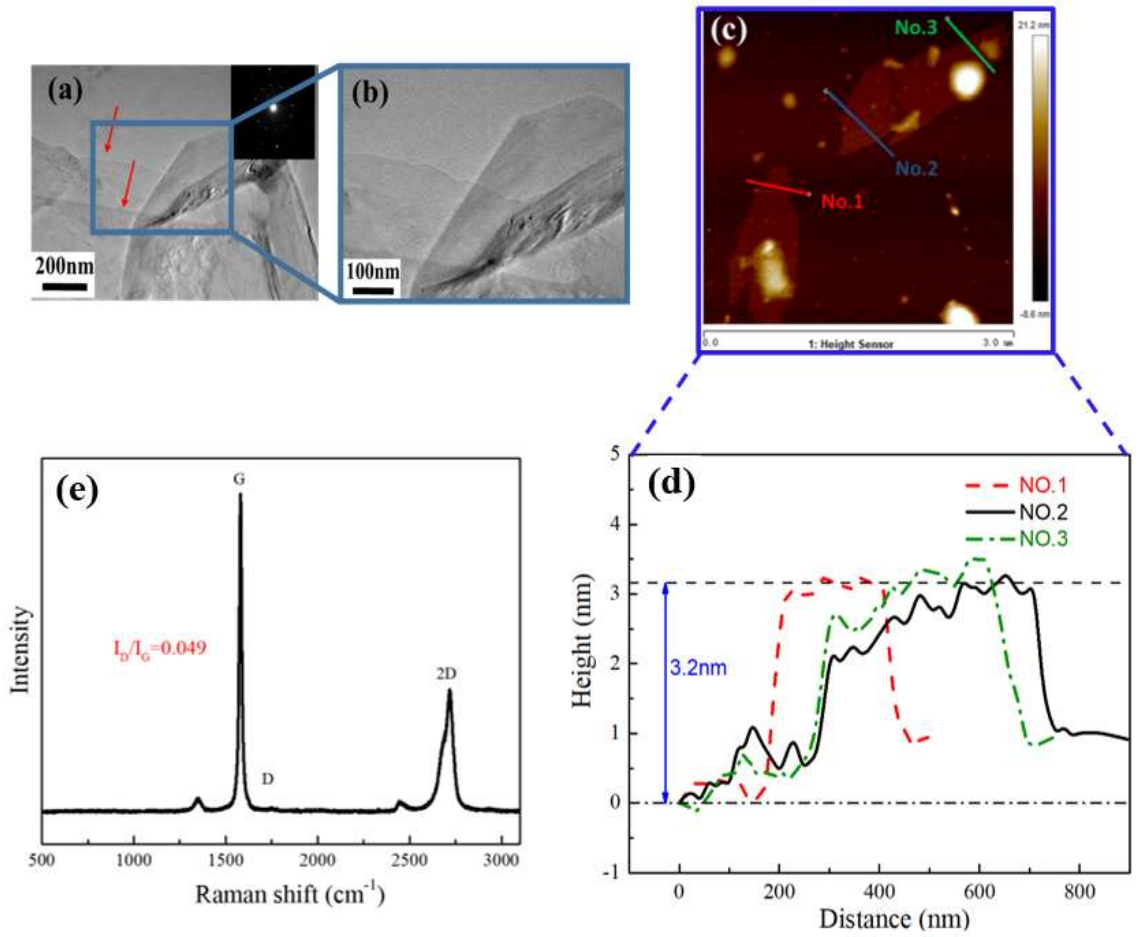

Figure 2. (a&b) TEM micrographs of graphene platelets (c, d) AFM micrograph and thickness (height) of randomly selected graphene platelets and (e) Raman spectrum of graphene platelets.

3.2. Powder morphology of aluminum alloy and its GnP composites

Figure 3 shows the micrographs by SEM of pure Al-alloy ($AlSi_7Mg$) powder and its 0.05 and 0.1 wt% GnP-based nanocomposites after 16 hours of ball milling. Images (a, c and e) are in low magnification (600X) to observe the overall surface structure of the powders while Images (b, d and f) are captured at high magnification (20,000X) to further investigate the surface structure of each corresponding powder particles. The particle size range is 100–150 μm as depicted in Images (a, c and e). The pure $AlSi_7Mg$ alloy powders in Image (a) shows typical surface structure of pure Al powder with good sphericity [39]. When a small area is magnified to Image (b), a uniformly distributed small protrusions are observed, which is related to the atomization process of the Al alloy.

When Al-alloy powder is roll-milled with GnPs for 16 hours at different GnP fractions, the Al-alloy

powder surface becomes rough yet spherical. At 0.05 wt%, Image (c) illustrates that GnPs homogeneously and completely cover the particles resulting in rough Al alloy/GnP surface powders. Obviously, the Al-alloy/GnP powder in Image (c) retains its spherical shape after ball-milling which means that GnPs are possible physically attached to Al-alloy powder surface and/or attached by chemical bonding such as van der Waal's forces without the hydrolysis reaction. Zhang L. *et al* [16] ball-milled pure aluminum powder with graphene oxide (GO) in deionized (DI) water and dried. The authors found that Al/GO powder shape transformed from spherical into irregular shape due to the hydrolysis reaction occurred during the drying process. It is noteworthy to mention that the Al/GO powder kept its spherical shape when they were rinsed by alcohol, then dried. When GnPs were added at 0.1 wt% to Al-alloy powder and ball-milled, the composite-powder surface becomes rougher with thick GnPs attached to Al-alloy powder as shown in Image (e) and (f). From Image (e), it seems that GnPs erode the Al-alloy particle during the ball milling process at high fractions (yellow circles); graphene is the stiffest and strongest material ever measured and hence possesses extremely high hardness while Al-alloy is soft and ductile material. Due to friction between steel-balls, Al-alloy powder and GnPs, the GnPs will erode Al-alloy powder in the course of ball-milling process. This is paramount at high GnPs. In general, composite powder in spherical or near spherical shape benefits the LDM process in 3D-printing high density metal composite [40].

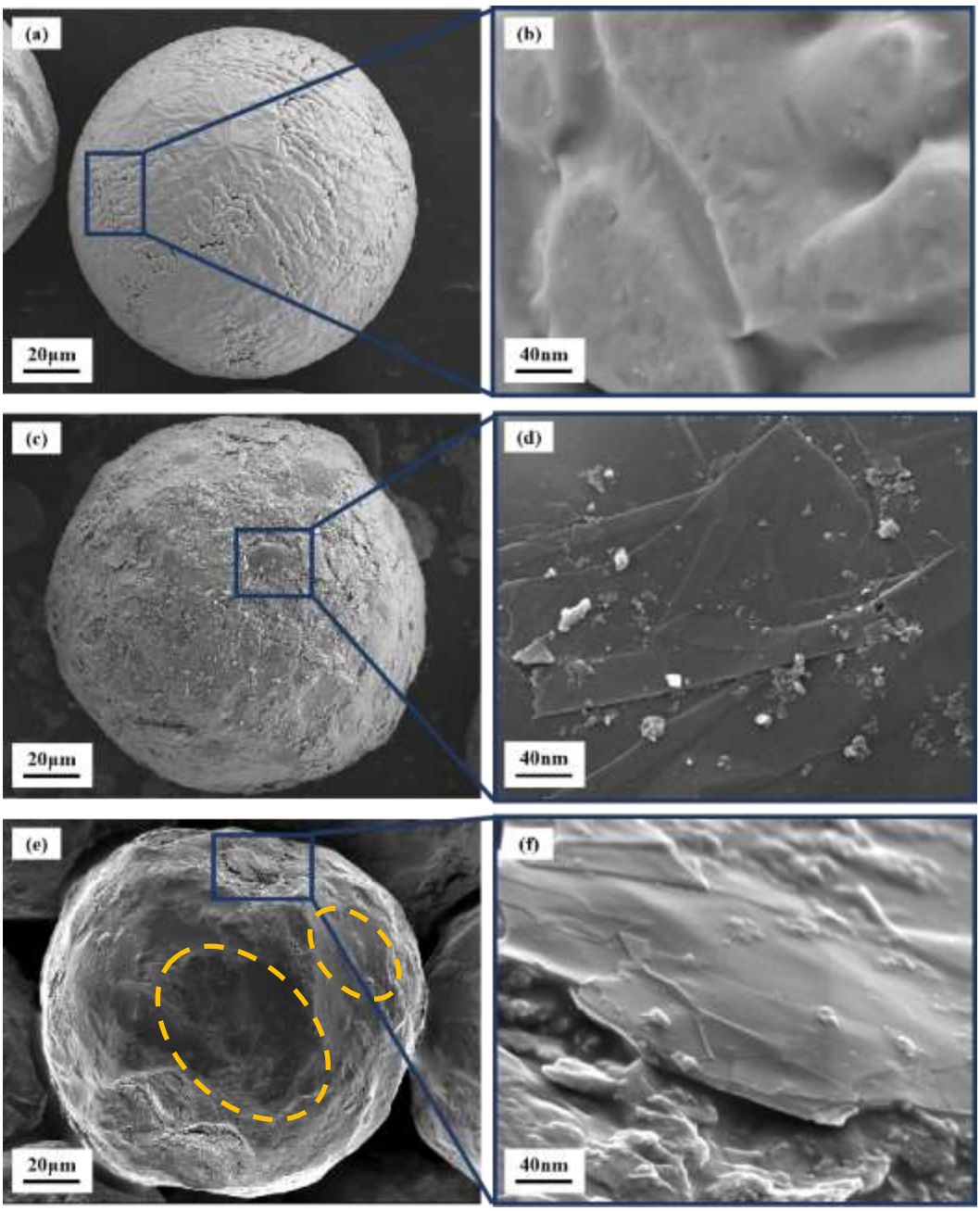

Figure 3. SEM images of (a, c and e) pure Al-alloy, 0.05wt% and 0.1 wt% composites at low magnifications; and (b, d and f) images of the above fractions at high magnification; respectively

Figure 4 shows optical micrographs of the metallographic structure of pure Al-alloy and its GnP's nanocomposites prepared by LDM process. The white gray coloured areas are assigned to primary α-Al dendrite (yellow arrows) while the dark areas correspond to eutectics of (α-Al + Si) [41] as highlighted by red-coloured contours. It is evident in Figure 4 that the inclusion of GnPs into Al-alloy through LDM process changes the metallographic structure of the Al-alloy. Figure 4b &c shows that the grain size and range of grain distribution of the composite are significantly smaller than that of

pure Al-alloy in Figure 4a. At the same time, with the increase of GnP content, the number of near-circular grains increases; this indicates that GnPs are effective in refining the $AlSi_7Mg$ alloy. Image-Pro Plus software was utilized to measure and calculate the grain size of the composite; it revealed that 0.05 wt% of GnPs refines the grain size from 18.2 to 11.8 μm. When the content of GnPs is increased to 0.1%, the average grain size reduced to 7.9 μm. These data indicate that grain refinement is pronounced with the increase of GnP content. According to the heterogeneous nucleation theory, GnPs can work as nucleation cores during solidification of aluminum alloy and hence form large number of small crystals. In the subsequent growth process, they collide with each other and their growth space is suppressed. With the increase of GnP content, more nucleation will be formed; this will effectively inhibit the growth of dendritic and obtain fine microstructure.

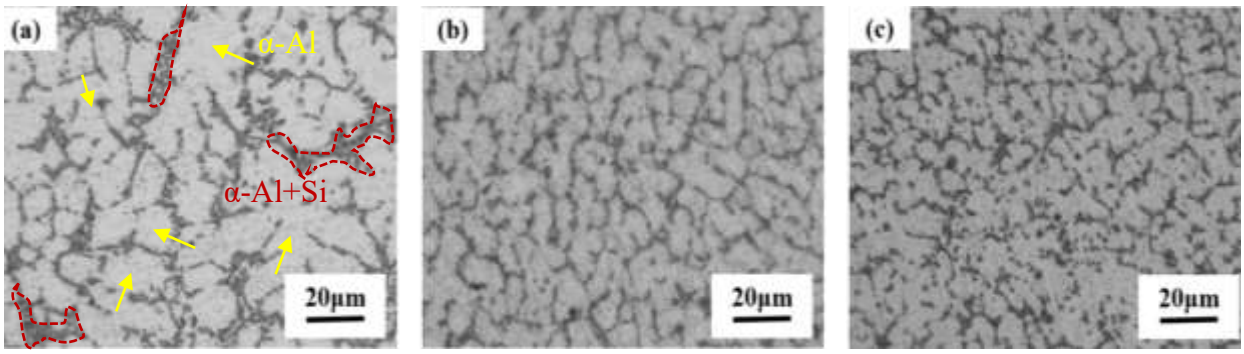

Figure 4. Optical microscopy images of (a) pure Al alloy, and (b) and (c) 0.05 and 0.1 wt% Al-alloy/GnP composite, respectively

Further morphological investigation was conducted by taking TEM micrographs for as Al-alloy/GnP nanocomposites as presented in Figure 5. Traces of GnPs indicated by yellow arrows are observed in Figure 5a. Also, few hexagonal structures of aluminum carbide (Al_4C_3) were depicted by blue arrows in Figure 5a. Aluminum carbide in carbon-based filler/aluminum alloy is inevitable and largely depends on the processing temperature and time. The free energy of Al_4C_3 is -168 kJ/mole at temperature range 650–750°C [42, 43]. In LDM, the temperature at the incident point of the laser beam is above 750°C which favours the formation of Al_4C_3. However, the laser beam is a focused

heat source which heats a narrow area of the powder at-a-time and then moves away– unlike to other processing methods such sintering. Short time of heating and small molten area does not form large quantity of Al_4C_3 [44].

The existence of Al_4C_3 in Al composites is a two-fold sword; excessive amount of Al_4C_3 deteriorates the mechanical performance of Al composites. On the other side, certain amount of it would improve the wettability between graphene platelets and Al-alloy matrix and hence strengthen interface between GnPs and Al-matrix leading to high mechanical strength. Figure 5c shows the EDS analysis results at point hexagonal area confirming the formation of Al_4C_3[45].

Figure 5d shows Raman spectrum of pure Al-alloy and its GnPs nanocomposites prepared by LDM 3D printing. Typical absorbance at ~1335, ~1580 and ~2673 cm^{-1} assigned to D, G and 2D bands of graphene platelets, respectively. In comparison with the Raman spectrum of graphene platelets in Figure 2e, the I_D/I_G of Al-alloy/GnP nanocomposite is significantly higher: I_D/I_G (0.05 wt% GnPs) < I_D/I_G (0.10 wt% GnPs). During the laser deposition process, thermal accumulation induced by the laser beam to the graphene structure increases structure defects in graphene. Also, the reaction between graphene and aluminum may increase structural defects. Similar results were observed by Hu Z. *et al* [28]; they reported I_D/I_G of 0.48 for Al/graphene nanocomposite prepared by selective laser melting, in comparison with 0.053 for graphene.

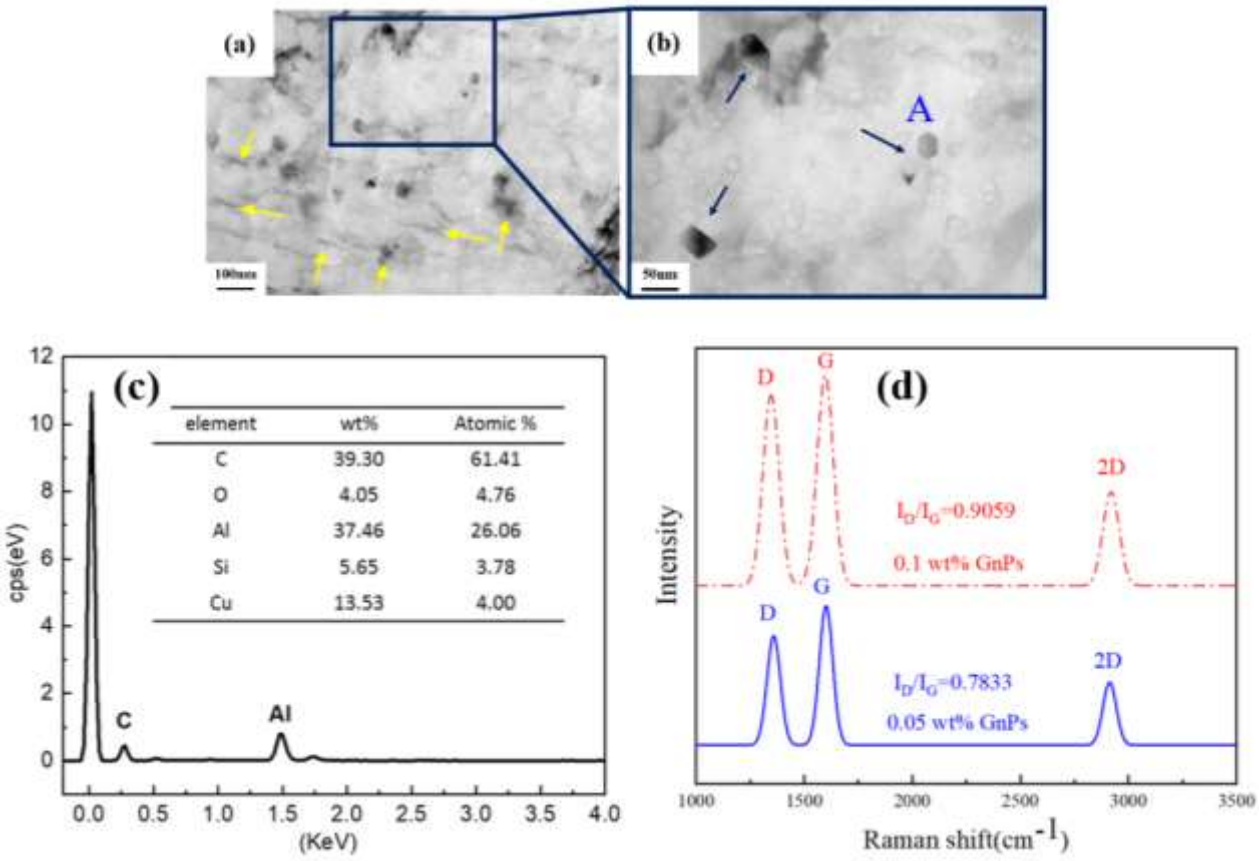

Figure 5. (a, b) TEM micrographs of 3D-printed Al-alloy/GnP nanocomposite, (c) energy dispersive spectrum (EDS) at point A and (d) Raman spectra of 3D-printed Al-alloy/GnP nanocomposites.

3D-printed Al-alloy/GnP composite samples were cut, polished and then examined using x-ray diffraction (XRD) to investigate their phase composition. Figure 6 displays the XRD patterns of pure Al-alloy, and 0.05 and 0.1 wt% of Al-alloy/GnP composites. The XRD analysis revealed that the composition of the 3D-printed composites comprises of Al and Si. The *2θ* peaks at 38.472°,44.738°, 65.133°, 78.227°, and 82.435° are associated to (111), (200), (220) (311) and (222) crystal planes of Al according to PDF #04-0787 [46]. Other peaks can be found at *2θ* of 28.442°, 47.302°, and 56.121° which are indexed to (111), (220) and (311) crystal planes of Si according to PDF #27-1402. Due to the low fraction of GnP in the fabricated Al-alloy composites, XRD was not able to capture peaks for graphene.

The formation of aluminum carbide (Al_4C_3) at the interface between GnPs and Al-alloy matrix is crucial; Al_4C_3 is a brittle compound and promote the phase separation in the fabricated composite

leading to low mechanical performance. According to PDF#35-0799, Al_4C_3 phase can be detected at *2θ* peaks of 31.13°, 31.77°, 35.89°, 40.12° and 55.05° which were not observed in Figure 6. This means that Al_4C_3 was not detected by XRD test. However, TEM micrographs showed some hexagonal structures within the Al-alloy matrix. This suggests the quantity of Al_4C_3 was minimal endowing another advantage of LDM-processed Al-alloy/graphene nanocomposite. The $AlSi_7Mg$ alloy contains (0.45–0.6 wt%) Mg and (6.5–7.5 wt%) Si as summarized in Table 1; it was reported that Mg and Si are alloying elements which minimize the formation of Al_4C_3 at the interface between GnPs and Al alloy [47]. Although the mechanism of suppressing the formation of Al_4C_3 at the interface by Mg content is not fully understood, Wang *et al.*[48] suggests that the existence of Mg promotes the formation of Al_3Mg_2 at the interface reducing the chance of having Al_4C_3. In the current study, the XRD patterns showed no needle-like Al_4C_3 leading to Al-alloy/GnP nanocomposites with high mechanical performance as elaborated in Section 3.4.

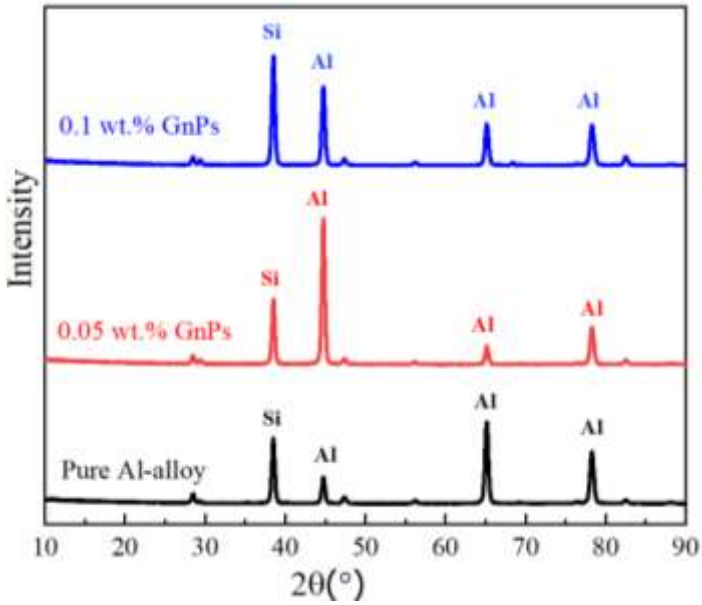

Figure 6. XRD patterns of the 3D printed pure Al alloy, and its GnP nanocomposites

3.3. Mechanical performance of the composites

The tensile strength, Young's modulus and elongation at break of pure Al-alloy and its GnP-based

composites as function of graphene content are shown in Figure 7. Evidently, GnPs possess significant reinforcing effect on Al-alloy; tensile strength and Young's modulus of the 3D-printed Al-alloy/GnP composites steadily increased with the GnP content. 0.1 wt% of GnP increases the tensile strength and Young's modulus of pure Al-alloy from 149.7 to 240.5 MPa and 72.5 to 89.2 GPa recording 60.7% and 23.0% increments, respectively. Strikingly, in Figure 7d, the elongation at break of Al-alloy/GnP composites was increased by 193.7%. The literature reports that most of Al composites exhibit reductions in ductility upon adding stiff fillers such as graphene [1, 46, 47, 49-51]. This gives advantage to LDM 3D printing of producing Al/graphene nanocomposites with improvements in conflicting properties including tensile strength and Young's modulus, and elongation at break.

In addition to tensile testing, Vickers hardness test was performed on the LDM-processed Al/GnP composites. The average Vickers hardness values of these samples were plotted in Figure 7e; at 0.1 wt%, the Vickers hardness of Al-alloy/GnP composites enhanced by 66% in comparison with pure Al-alloy. Liu J. *et al* [15] reported 43% increment when 0.15 wt% graphene sheets are added to Al by compacting and sintering. In another study, 0.1wt% Al/graphene oxide composite exhibited 14% increment in Vickers hardness as the composites were produced by powder metallurgy technique [16].

The high mechanical performance of Al-alloy upon adding GnPs using LDM is due to the following factors: (i) the high contrast in strength and Young's modulus between graphene and Al-alloy endows Al-alloy ability to effectively resist mechanical load along with the good interface between the two phases [52]; (ii) GnPs have assured uniform dispersion within the Al-alloy matrix by LDM because they have attached to and coated Al-alloy powder during ball-milling process, thus GnPs do not work as stress concentration centres and could assist the matrix in resisting mechanical load; (iii) the

significant thermal expansion coefficient mismatch between GnP and Al-alloy leads to high dislocation density at the interface resulting in high strength [53]; GnPs could also work as a barrier so that dislocations do not freely move through the matrix [17, 53]; (iv) the absence of needle-like structure Al_3C_4 at the GnPs and Al-alloy interface promotes very much the ductility of the Al composite; and (v) existence of GnPs restrains the growth of Al grains during fabrication of the composites bringing on grain refinement strengthening mechanism [54, 55].

On the other hand, when graphene platelets content increased to 0.2 wt%, the increments in tensile strength and elongation at break drop though they are still higher than pure Al-alloy; Young's modulus of 0.2 wt% Al-alloy/GnP nanocomposite less than pure Al-alloy. This is assigned to two main reasons: agglomeration of GnPs and formation of large quantity of Al_3C_4. The later induces crack initiation due to stress concentration while the former factor promotes phase separation.

It is generally known that the mechanical properties of the composites are dominated not only by the reinforcement and the matrix but also by the interfacial bonding strength between them[56]. It is necessary to study the materials fracture behaviour to understand the load transfer between the matrix and reinforcement. Improvements in the strength of Al-alloy/graphene composites are mainly attributable to the effective load transfer between the matrix and graphene through the interface. Good load transfer is the reason for the basic toughening mechanism of GnPs [57-59]. It is seen from Figure 8 that the graphene platelets are uniformly distributed in the matrix; meanwhile, some platelets are pulled-out and observed on the tensile fracture surfaces of 3D printed Al-alloy/GnP nanocomposites. The pits on the fracture surface indicate that the length of the graphene pulled-out are very short, suggesting a strong interfacial bonding between graphene and the Al matrix. This also indicates that the high mechanical properties are obtained in 0.1wt.% graphene/ AlSi7Mg composite. Figure 8

shows a graphene is bonding to the Al matrix in “bridging” manner, increasing the Al–GnPs interface strength and the fracture energy of the composites.

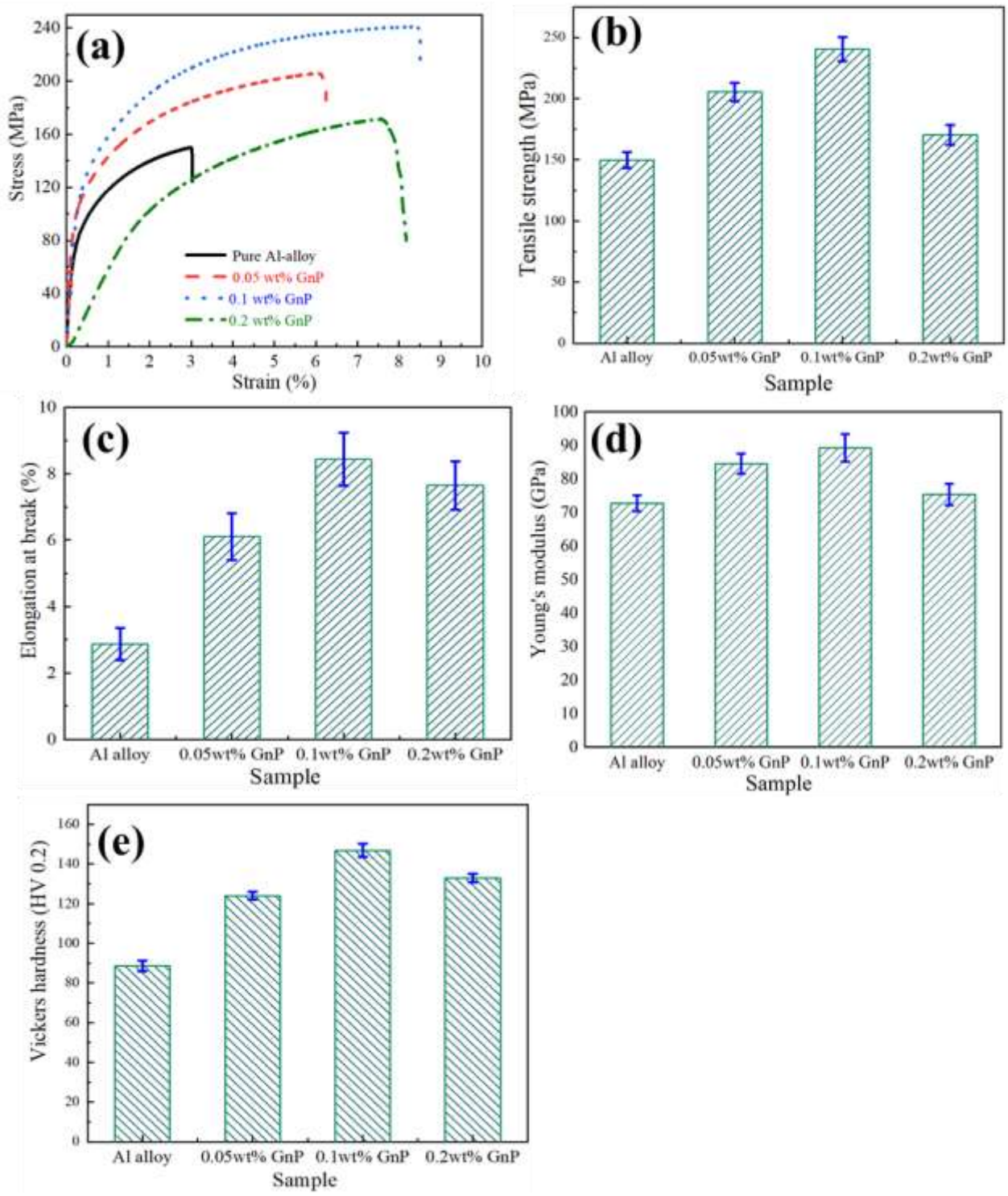

Figure 7. Mechanical performance of pure Al-alloy and its GnPs- nanocomposites: (a) stress-strain curve, (b) tensile strength, (c) elongation at break, (d) Young’s moduli and (e)Vickers Hardness

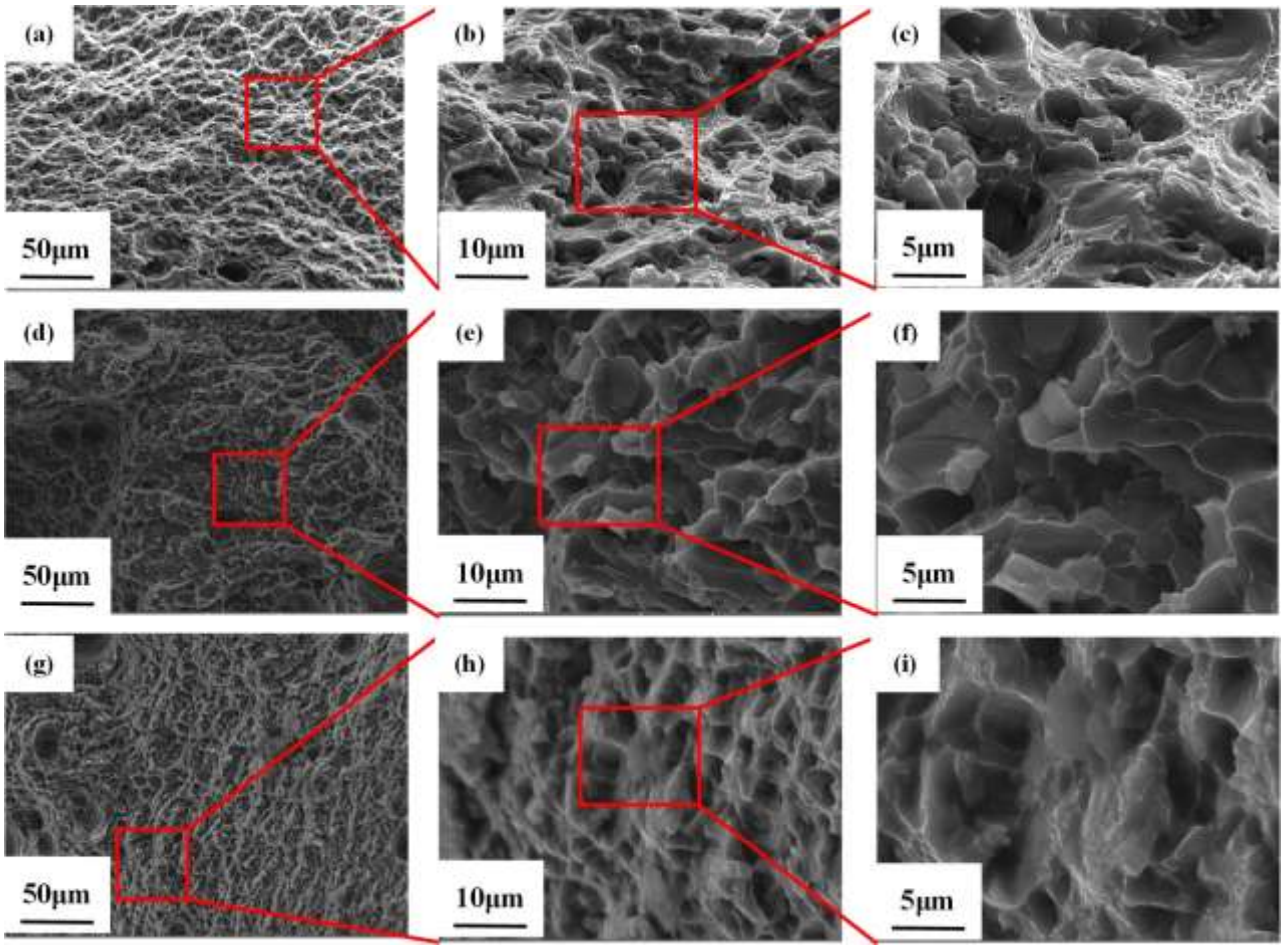

Figure 8.Fracture morphology of composites (a-c) pure al alloy,(d-f) 0.05 wt% Al-alloy/GnP composite, (g-i) 0.1 wt% Al-alloy/GnP composite

Table 2 summarizes the mechanical performance of Al/graphene nanocomposites prepared by different methods [28, 40, 60-63]. It is evident that method of fabrication is a key factor in determining mechanical properties of Al composites. Generally, tensile strength and hardness of Al composites increase with the graphene content. SLM – one of 3D printing methods – [28, 40, 60] did not show significant improvements in tensile strength, hardness and elongation at break in comparison with traditional fabrication methods such as powder metallurgy and frication stir processing [62, 63]. For example, 1 wt% of graphene into Al alloy via SLM increased tensile strength by 11% while it was incremented by 23.3% when stir friction method was used. It is worth noting that the composite materials obtained by traditional processing methods have a great loss of toughness while increasing

the strength; for example, 1.5 wt% graphene reduced toughness of the Al alloy by 60% when field activated and pressure assisted synthesis (FAPAS) was employed [61]. In addition, the traditional processing methods are not flexible to form complex parts. SLM method as an additive manufacturing is able to create intricate shapes with no loss in toughness (even improved) though tensile strength is not as high as desired. The current study evidenced that LDM method is able to solve and overcome the aforementioned disadvantages of both SLM and traditional fabrication methods due to the advantage of using coaxial powder feeding in LDM[64]. In our work, tensile strength and simultaneously elongation at break were exceedingly increased by 60.7% and 193%; elongation at break is an indirect indicator for toughness.

Table 2.Comparison of mechanical performance

Synthesis method	Graphene content (wt%)	Tensile strength (MPa)	Elongation (%)	Hardness (HV)	Reference
Ball milling and 3D printing, LDM	0 / 0.05 / 0.1	149.7 / 205.43 / 240.49 (66.7% increase)	2.87 / 6.1 / 8.43 (193.7% increase)	88.63 / 124.98 / 146.87 (66% increase)	Our study
Ball milling and SLM	0 / 1	357 / 396 (11% increase)	5.5 / 6.2 (13% increase)	120 / 169 (40.8% increase)	[40]
Ball milling and SLM	0 / 0.5 / 1 / 2.5	N/A	N/A	38 / 47.1 / 49.6 / 66.6 (75.3% increase)	[28]
Ball milling and SLM	0 / 0.5	337 / 346 (2.67% increase)	3.0 / 3.2 (6.67% increase)	N/A	[60]
FAPAS	0 / 0.5 / 1 / 1.5	91 / 131 / 115 / 104 (44%,26% and 14% increase)	60 / 42 / 34 / 24 (30%,43% and 60% decrease)	N/A	[61]
Powder metallurgy and frication stir processing	0 / 1	417 / 514 (23.3% increase)	12 / 10 (16.6% decrease)	N/A	[62]
Solution mixing and powder metallurgy	0 / 0.3 / 0.6	203 / 255 / 241 (25% and 18% increase)	30.5 / 19.2 / 13.2 (37% and 56.7% decrease)	59.1 / 74.3 / 71.3 (25.7% and 20.6% increase)	[63]

SLM: selective laser melting; FAPAS: field activated and pressure assisted synthesis

Conclusion

In this paper, graphene platelets (GnPs) at various fractions were successfully added into aluminum alloy by 3D printing technology – laser deposition manufacturing (LDM). Comprehensive morphological and mechanical performance measurements were employed to investigate structure-property relations of Al-alloy/GnP nanocomposites. AFM revealed that the produced GnPs possessed an average thickness of 3.2 ± 0.7nm which are of high structural integrity as confirmed by the I_D/I_G of 0.049 from Raman analysis. TEM analysis for Al-alloy/GnP nanocomposites showed that GnPs uniformly distributed; Al_4C_3 was observed in hexagonal shapes with no sign of having needle-like structure. Small quantity of Al_4C_3 could promote the wettability of GnPs into Al matrix leading to good interface and high mechanical performance. Surprisingly, Al-alloy/GnP nanocomposites prepared by LDM process have outstanding increments in tensile strength, hardness and elongation at break; they were increased by 67%, 66% and 193%, respectively at 0.1 wt% GnPs. To the best of our knowledge, this is the first time to report such ductile Al/GnP nanocomposites and yet possess high strength and stiffness. These properties started to decrease at 0.2 wt% GnPs mainly due to graphene agglomeration and formation of more Al_4C_3.

The study indicates that laser deposition manufacturing (LDM) is a promising process not only for aluminum/graphene nanocomposites but also for other metallic nanocomposites; since it is an additive manufacturing process, it is capable to produce intricate profiles which traditional processes cannot make.

Acknowledgement

This work was financially supported by the Open Fund of Key Laboratory of Fundamental Science for Aeronautical Digital Manufactuing Process of Shenyang Aerospace University (SHSYS201905)

and the plan of rejuvenating the Talents of Liaoning Province (XLYC1907135).

References

[1] F. Chen, N. Gupta, R.K. Behera, P.K. Rohatgi, Graphene-Reinforced Aluminum Matrix Composites: A Review of Synthesis Methods and Properties, JOM, 70 (2018) 837-845.
[2] D.B. Miracle, Metal matrix composites – From science to technological significance, Composites Science and Technology, 65 (2005) 2526-2540.
[3] R. Jamaati, M.R. Toroghinejad, Manufacturing of high-strength aluminum/alumina composite by accumulative roll bonding, Materials Science and Engineering: A, 527 (2010) 4146-4151.
[4] C. Gao, W. Wu, J. Shi, Z. Xiao, A.H. Akbarzadeh, Simultaneous enhancement of strength, ductility, and hardness of TiN/AlSi10Mg nanocomposites via selective laser melting, Additive Manufacturing, 34 (2020) 101378.
[5] S. Han, Q. Meng, Z. Qiu, A. Osman, R. Cai, Y. Yu, T. Liu, S. Araby, Mechanical, toughness and thermal properties of 2D material- reinforced epoxy composites, Polymer, 184 (2019) 121884.
[6] S. Araby, X. Su, Q. Meng, H.-C. Kuan, C.-H. Wang, A. Mouritz, A. Maged, J. Ma, Graphene platelets versus phosphorus compounds for elastomeric composites: flame retardancy, mechanical performance and mechanisms, Nanotechnology, 30 (2019) 385703.
[7] G. Shi, S. Araby, C.T. Gibson, Q. Meng, S. Zhu, J. Ma, Graphene Platelets and Their Polymer Composites: Fabrication, Structure, Properties, and Applications, Advanced Functional Materials, 28 (2018) 1706705.
[8] S. Araby, N. Saber, X. Ma, N. Kawashima, H. Kang, H. Shen, L. Zhang, J. Xu, P. Majewski, J. Ma, Implication of multi-walled carbon nanotubes on polymer/graphene composites, Materials & Design (1980-2015), 65 (2015) 690-699.
[9] H. Porwal, S. Grasso, M.J. Reece, Review of graphene–ceramic matrix composites, Advances in Applied Ceramics, 112 (2013) 443-454.
[10] P. Miranzo, M. Belmonte, M.I. Osendi, From bulk to cellular structures: A review on ceramic/graphene filler composites, Journal of the European Ceramic Society, 37 (2017) 3649-3672.
[11] J. Ma, Q. Meng, I. Zaman, S. Zhu, A. Michelmore, N. Kawashima, C.H. Wang, H.-C. Kuan, Development of polymer composites using modified, high-structural integrity graphene platelets, Composites Science and Technology, 91 (2014) 82-90.
[12] Q. Meng, H. Wu, Z. Zhao, S. Araby, S. Lu, J. Ma, Free-standing, flexible, electrically conductive epoxy/graphene composite films, Composites Part A: Applied Science and Manufacturing, 92 (2017) 42-50.
[13] A.K. Geim, K.S. Novoselov, The rise of graphene, Nature Materials, 6 (2007) 183-191.
[14] A.K. Geim, Graphene: status and prospects, science, 324 (2009) 1530-1534.
[15] J. Liu, U. Khan, J. Coleman, B. Fernandez, P. Rodriguez, S. Naher, D. Brabazon, Graphene oxide and graphene nanosheet reinforced aluminium matrix composites: Powder synthesis and prepared composite characteristics, Materials & Design, 94 (2016) 87-94.
[16] L. Zhang, G. Hou, W. Zhai, Q. Ai, J. Feng, L. Zhang, P. Si, L. Ci, Aluminum/graphene composites with enhanced heat-dissipation properties by in-situ reduction of graphene oxide on aluminum particles, Journal of Alloys and Compounds, 748 (2018) 854-860.
[17] A. Fadavi Boostani, S. Tahamtan, Z.Y. Jiang, D. Wei, S. Yazdani, R. Azari Khosroshahi, R. Taherzadeh Mousavian, J. Xu, X. Zhang, D. Gong, Enhanced tensile properties of aluminium matrix composites reinforced with graphene encapsulated SiC nanoparticles, Composites Part A: Applied Science and Manufacturing, 68 (2015) 155-163.
[18] D. Gu, X. Rao, D. Dai, C. Ma, L. Xi, K. Lin, Laser additive manufacturing of carbon nanotubes (CNTs)

reinforced aluminum matrix nanocomposites: Processing optimization, microstructure evolution and mechanical properties, Additive Manufacturing, 29 (2019) 100801.
[19] C. Chen, Y. Xie, X. Yan, M. Ahmed, R. Lupoi, J. Wang, Z. Ren, H. Liao, S. Yin, Tribological properties of Al/diamond composites produced by cold spray additive manufacturing, Additive Manufacturing, 36 (2020) 101434.
[20] J.K. Tiwari, A. Mandal, N. Sathish, A.K. Agrawal, A.K. Srivastava, Investigation of porosity, microstructure and mechanical properties of additively manufactured graphene reinforced AlSi10Mg composite, Additive Manufacturing, 33 (2020) 101095.
[21] K.M.M. Billah, F.A.R. Lorenzana, N.L. Martinez, R.B. Wicker, D. Espalin, Thermomechanical characterization of short carbon fiber and short glass fiber-reinforced ABS used in large format additive manufacturing, Additive Manufacturing, 35 (2020) 101299.
[22] N. van de Werken, H. Tekinalp, P. Khanbolouki, S. Ozcan, A. Williams, M. Tehrani, Additively manufactured carbon fiber-reinforced composites: State of the art and perspective, Additive Manufacturing, 31 (2020) 100962.
[23] G. Wu, Z. Yu, L. Jiang, C. Zhou, G. Deng, X. Deng, Y. Xiao, A novel method for preparing graphene nanosheets/Al composites by accumulative extrusion-bonding process, Carbon, 152 (2019) 932-945.
[24] Y. Wu, K. Zhan, Z. Yang, W. Sun, B. Zhao, Y. Yan, J. Yang, Graphene oxide/Al composites with enhanced mechanical properties fabricated by simple electrostatic interaction and powder metallurgy, Journal of Alloys and Compounds, 775 (2019) 233-240.
[25] M.E. Turan, Investigation of mechanical properties of carbonaceous (MWCNT, GNPs and C60) reinforced hot-extruded aluminum matrix composites, Journal of Alloys and Compounds, 788 (2019) 352-360.
[26] T. Chen, Y.-C. Lin, Feasibility Evaluation and Optimization of a Smart Manufacturing System Based on 3D Printing: A Review, International Journal of Intelligent Systems, 32 (2017) 394-413.
[27] Z. Hu, F. Chen, D. Lin, Q. Nian, P. Parandoush, X. Zhu, Z. Shao, G.J. Cheng, Laser additive manufacturing bulk graphene–copper nanocomposites, Nanotechnology, 28 (2017) 445705.
[28] Z. Hu, F. Chen, J. Xu, Q. Nian, D. Lin, C. Chen, X. Zhu, Y. Chen, M. Zhang, 3D printing graphene-aluminum nanocomposites, Journal of Alloys and Compounds, 746 (2018) 269-276.
[29] Z. Hu, D. Wang, C. Chen, X. Wang, X. Chen, Q. Nian, Bulk titanium–graphene nanocomposites fabricated by selective laser melting, Journal of Materials Research, 34 (2019) 1744-1753.
[30] Z. Hu, Y. Li, X. Fan, F. Chen, J. Xu, Mechanical and tribological property of single layer graphene oxide reinforced titanium matrix composite coating, AIP Conference Proceedings, 1955 (2018) 020014.
[31] Y. Hu, W. Cong, A review on laser deposition-additive manufacturing of ceramics and ceramic reinforced metal matrix composites, Ceramics International, 44 (2018) 20599-20612.
[32] G. Shi, S.E. Lowe, A.J.T. Teo, T.K. Dinh, S.H. Tan, J. Qin, Y. Zhang, Y.L. Zhong, H. Zhao, A versatile PDMS submicrobead/graphene oxide nanocomposite ink for the direct ink writing of wearable micron-scale tactile sensors, Applied Materials Today, 16 (2019) 482-492.
[33] T.-C. Lin, C. Cao, M. Sokoluk, L. Jiang, X. Wang, J.M. Schoenung, E.J. Lavernia, X. Li, Aluminum with dispersed nanoparticles by laser additive manufacturing, Nature Communications, 10 (2019) 4124.
[34] S. Han, A. Chand, S. Araby, R. Cai, S. Chen, H. Kang, R. Cheng, Q. Meng, Thermally and electrically conductive multifunctional sensor based on epoxy/graphene composite, Nanotechnology, 31 (2019) 075702.
[35] I. Zaman, H.-C. Kuan, Q. Meng, A. Michelmore, N. Kawashima, T. Pitt, L. Zhang, S. Gouda, L. Luong, J. Ma, A Facile Approach to Chemically Modified Graphene and its Polymer Nanocomposites, Advanced Functional Materials, 22 (2012) 2735-2743.
[36] Q. Meng, S. Araby, J. Ma, Toughening mechanisms in epoxy/graphene platelets composites, in: Toughening Mechanisms in Composite Materials, 2015, pp. 73-112.

[37] A.C. Ferrari, J. Meyer, V. Scardaci, C. Casiraghi, M. Lazzeri, F. Mauri, S. Piscanec, D. Jiang, K. Novoselov, S. Roth, A.K. Geim, Raman Spectrum of Graphene and Graphene Layers, Physical review letters, 97 (2006) 187401.
[38] M.S. Dresselhaus, A. Jorio, A.G.S. Filho, R. Saito, Defect characterization in graphene and carbon nanotubes using Raman spectroscopy, Philosophical Transactions of the Royal Society A: Mathematical, Physical and Engineering Sciences, 368 (2010) 5355-5377.
[39] B. Vautherin, M.P. Planche, R. Bolot, A. Quet, L. Bianchi, G. Montavon, Vapors and Droplets Mixture Deposition of Metallic Coatings by Very Low Pressure Plasma Spraying, Journal of Thermal Spray Technology, 23 (2014) 596-608.
[40] Z. Zhao, P. Bai, R.D.K. Misra, M. Dong, R. Guan, Y. Li, J. Zhang, L. Tan, J. Gao, T. Ding, W. Du, Z. Guo, AlSi10Mg alloy nanocomposites reinforced with aluminum-coated graphene: Selective laser melting, interfacial microstructure and property analysis, Journal of Alloys and Compounds, 792 (2019) 203-214.
[41] K. Kang, D. Li, G. Gao, A. Wang, D. Shi, Effect of Electric Pulse Current Rapid Aging Treatment on Microstructure and Properties of Al-7Si-0.55Mg Alloy, Metals, 9 (2019) 1103.
[42] S.F. Bartolucci, J. Paras, M.A. Rafiee, J. Rafiee, S. Lee, D. Kapoor, N. Koratkar, Graphene–aluminum nanocomposites, Materials Science and Engineering: A, 528 (2011) 7933-7937.
[43] T. Etter, P. Schulz, M. Weber, J. Metz, M. Wimmler, J.F. Löffler, P.J. Uggowitzer, Aluminium carbide formation in interpenetrating graphite/aluminium composites, Materials Science and Engineering: A, 448 (2007) 1-6.
[44] Y. Jiang, Z. Tan, G. Fan, Z. Zhang, D.-B. Xiong, Q. Guo, Z. Li, D. Zhang, Nucleation and growth mechanisms of interfacial carbide in graphene nanosheet/Al composites, Carbon, 161 (2020) 17-24.
[45] G. Li, Y. Qu, Y. Yang, R. Chen, Q. Zhou, R. Li, Effect of mechanical combined with electromagnetic stirring on the dispersity of carbon fibers in the aluminum matrix, Scientific Reports, 10 (2020) 8106.
[46] P. Shao, W. Yang, Q. Zhang, Q. Meng, X. Tan, Z. Xiu, J. Qiao, Z. Yu, G. Wu, Microstructure and tensile properties of 5083 Al matrix composites reinforced with graphene oxide and graphene nanoplates prepared by pressure infiltration method, Composites Part A: Applied Science and Manufacturing, 109 (2018) 151-162.
[47] J. Pelleg, D. Ashkenazi, M. Ganor, The influence of a third element on the interface reactions in metal–matrix composites (MMC): Al–graphite system, Materials Science and Engineering: A, 281 (2000) 239-247.
[48] C. Wang, G. Chen, X. Wang, Y. Zhang, W. Yang, G. Wu, Effect of Mg Content on the Thermodynamics of Interface Reaction in Cf/Al Composite, Metallurgical and Materials Transactions A, 43 (2012) 2514-2519.
[49] J. Wang, Z. Li, G. Fan, H. Pan, Z. Chen, D. Zhang, Reinforcement with graphene nanosheets in aluminum matrix composites, Scripta Materialia, 66 (2012) 594-597.
[50] S. Dixit, A. Mahata, D.R. Mahapatra, S.V. Kailas, K. Chattopadhyay, Multi-layer graphene reinforced aluminum – Manufacturing of high strength composite by friction stir alloying, Composites Part B: Engineering, 136 (2018) 63-71.
[51] J.G. Park, D.H. Keum, Y.H. Lee, Strengthening mechanisms in carbon nanotube-reinforced aluminum composites, Carbon, 95 (2015) 690-698.
[52] B. Xiong, K. Liu, W. Xiong, X. Wu, J. Sun, Strengthening effect induced by interfacial reaction in graphene nanoplatelets reinforced aluminum matrix composites, Journal of Alloys and Compounds, 845 (2020) 156282.
[53] M. Rashad, F. Pan, A. Tang, M. Asif, Effect of Graphene Nanoplatelets addition on mechanical properties of pure aluminum using a semi-powder method, Progress in Natural Science: Materials International, 24 (2014) 101-108.
[54] Z. Yu, Z. Tan, R. Xu, G. Ji, G. Fan, D.-B. Xiong, Q. Guo, Z. Li, D. Zhang, Enhanced load transfer by designing mechanical interfacial bonding in carbon nanotube reinforced aluminum composites, Carbon, 146

(2019) 155-161.
[55] B. Chen, K. Kondoh, J. Umeda, S. Li, L. Jia, J. Li, Interfacial in-situ Al2O3 nanoparticles enhance load transfer in carbon nanotube (CNT)-reinforced aluminum matrix composites, Journal of Alloys and Compounds, 789 (2019) 25-29.
[56] Y. Jiang, R. Xu, Z. Tan, G. Ji, G. Fan, Z. Li, D.-B. Xiong, Q. Guo, Z. Li, D. Zhang, Interface-induced strain hardening of graphene nanosheet/aluminum composites, Carbon, 146 (2019) 17-27.
[57] T. Wang, Y. Zhang, Q. Liu, W. Cheng, X. Wang, L. Pan, B. Xu, H. Xu, A Self-Healable, Highly Stretchable, and Solution Processable Conductive Polymer Composite for Ultrasensitive Strain and Pressure Sensing, Advanced Functional Materials, 28 (2018) 1705551.
[58] G. Shi, Z. Zhao, J.-H. Pai, I. Lee, L. Zhang, C. Stevenson, K. Ishara, R. Zhang, H. Zhu, J. Ma, Highly Sensitive, Wearable, Durable Strain Sensors and Stretchable Conductors Using Graphene/Silicon Rubber Composites, Advanced Functional Materials, 26 (2016) 7614-7625.
[59] I. Hwang, H.N. Kim, M. Seong, S.-H. Lee, M. Kang, H. Yi, W.G. Bae, M.K. Kwak, H.E. Jeong, Multifunctional Smart Skin Adhesive Patches for Advanced Health Care, Advanced Healthcare Materials, 7 (2018) 1800275.
[60] Y. Wang, J. Shi, Investigation of Porosity and Mechanical Properties of Graphene Nanoplatelets Reinforced AlSi10Mg by Selective Laser Melting, (2017).
[61] J. Wang, L.-n. Guo, W.-m. Lin, J. Chen, C.-l. Liu, S.-d. Chen, S. Zhang, T.-t. Zhen, Effect of the graphene content on the microstructures and properties of graphene/aluminum composites, New Carbon Materials, 34 (2019) 275-285.
[62] Z.W. Zhang, Z.Y. Liu, B.L. Xiao, D.R. Ni, Z.Y. Ma, High efficiency dispersal and strengthening of graphene reinforced aluminum alloy composites fabricated by powder metallurgy combined with friction stir processing, Carbon, 135 (2018) 215-223.
[63] X. Zeng, J. Teng, J.-g. Yu, A.-s. Tan, D.-f. Fu, H. Zhang, Fabrication of homogeneously dispersed graphene/Al composites by solution mixing and powder metallurgy, International Journal of Minerals, Metallurgy, and Materials, 25 (2018) 102-109.
[64] L. Aucott, H. Dong, W. Mirihanage, R. Atwood, A. Kidess, S. Gao, S. Wen, J. Marsden, S. Feng, M. Tong, T. Connolley, M. Drakopoulos, C.R. Kleijn, I.M. Richardson, D.J. Browne, R.H. Mathiesen, H.V. Atkinson, Revealing internal flow behaviour in arc welding and additive manufacturing of metals, Nature Communications, 9 (2018) 5414.